Surface & Coatings Technology 205 (2011) 5269–5277

Contents lists available at ScienceDirect

Surface & Coatings Technology

journal homepage: www.elsevier.com/locate/surfcoat

Effects of H_2 plasma treatment on properties of ZnO:Al thin films prepared by RF magnetron sputtering

Fang-Hsing Wang *, Hung-Peng Chang, Chih-Chung Tseng, Chia-Cheng Huang

Department of Electrical Engineering and Graduate Institute of Optoelectronic Engineering, National Chung Hsing University, Taichung, Taiwan, R.O.C.

ARTICLE INFO

Article history:
Received 11 December 2010
Accepted 18 May 2011
Available online 27 May 2011

Keywords:
Transparent conductive oxide
Al-doped ZnO
Sputtering
Thin film

ABSTRACT

Al-doped ZnO (AZO) thin films were prepared on glass substrates by radio-frequency magnetron sputtering at deposition temperatures ranging from room temperature (RT) to 300 °C for transparent electrode applications. This study investigates the effects of H_2 plasma treatment on structural, electrical, and optical properties of AZO thin films. Plasma treatment was conducted at 300 °C using a plasma-enhanced chemical vapor deposition system for potential large size substrate applications. The crystal structure of plasma treated AZO films did not change considerably, but the surface roughness and surface grain size increased slightly. Improvement in electrical properties was strongly dependent on the deposition temperature. When the deposition temperature ranged from 300 °C to RT, the resistivity of plasma treated films decreased significantly by 22.7% to 97.6%, and the optical bandgap broadened by 0.011 to 0.076 eV.

1. Introduction

Transparent conductive oxide (TCO) films are extensively used for a variety of applications due to their high visible transmittance and low resistivity [1]. Among the various TCO films, indium–tin-oxide (ITO) is commonly used for many applications [2–4]. However, indium has become increasingly expensive due to scarcity. Zinc oxide (ZnO) has attracted attention because of its abundance, non-toxicity, and relatively low cost [5–7]. ZnO has an n-type wide bandgap with a wurtzite crystal structure. The electrical conductivity of ZnO is primarily dominated by electrons generated by oxygen vacancies and Zn interstitial atoms [6,7]. However, undoped ZnO films have unstable electrical characteristics because the electrical resistivity of the films varies under oxygen chemisorption and desorption. Doping trivalent elements such as Al, In, and Ga can further improve ZnO resistivity [8–10]. The electrical conductivity and optical transparency of the doped-ZnO depend on the nature, number, and atomic arrangement of metal cations in the ZnO structure, and on the presence of intrinsic or extrinsic defects. Many recent studies examine aluminum-doped ZnO thin films as transparent electrodes in liquid-crystal displays (LCDs), plasma display panels (PDPs), organic-light-emitting-diode displays (OLEDs), and solar cells [8,11,12]. Besides, these films also find applications in infrared and heat reflectors [13], antistatic coatings [14], multifunctional ferromagnetic films [15], varistors [16], blue/UV light emitting devices [17], gas sensors [18], surface acoustic wave devices [19], etc.

Researchers have employed many deposition techniques to prepare AZO thin films, including chemical vapor deposition (CVD), spray pyrolysis, sol–gel process, pulsed laser deposition, and reactive sputtering [5–12,19–21]. Among these techniques, reactive sputtering has attracted great interest because of the inherent ease with which the deposition conditions can be controlled [9]. Sputtered AZO films are strongly oriented perpendicular to the substrate (c-axis orientation) and have a polycrystalline hexagonal wurtzite structure [22]. These films also have abundant raw material, good thermal stability, and better plasma stability in hydrogen ambient than ITO or F-doped tin oxide (FTO) films, and hence can serve as potential alternatives to ITO or FTO [8,23].

Deposition parameters influence the structural, electrical, and optical properties of AZO films [24–27]. Park et al. [25] investigated the effect of preparation conditions on the physical properties of AZO films, including the $A1_2O_3$ content in the target, RF power, substrate temperature, and working pressure. Li et al. [26] reported the effects of substrate temperature on the crystallization behavior and optical properties of ZnO and AZO films. However, the electrical conductivity of AZO films degrades when the films are exposed to air ambient [7] and requires additional enhancement for high-efficiency photovoltaic cell applications. To improve the properties of ZnO films, researchers have studied various post-treatment techniques, such as hydrogen annealing [28,29], hydrogen plasma exposure [7,30–34], hydrogen ion implantation [35], and addition of hydrogen in deposition process [36–38]. Oh et al. [29] proposed that the improved electrical properties of AZO films after hydrogen annealing were due to the desorption of negatively charged oxygen species from the grain boundary surfaces. Cai et al. [33] suggested that the hydrogen in the plasma treated ZnO film not only passivated most of defects and

* Corresponding author at: 250 Kuo-Kuang Rd., Taichung 40227, Taiwan. Tel.: +886 4 22851549x706; fax: +886 4 22851410.
E-mail address: fansen@dragon.nchu.edu.tw (F.-H. Wang).

0257-8972/$ – see front matter © 2011 Elsevier B.V. All rights reserved.
doi:10.1016/j.surfcoat.2011.05.033

acceptors, but also introduced shallow donor states such as the V_O–H complex and the interstitial hydrogen H_i. We previously reported the effects of H_2 plasma treatment on the physical properties of AZO films sputtered at different sputtering RF powers and H_2 plasma RF powers [39,40]. These results motivated us to further study the characteristics of H_2 plasma treated AZO films and the detailed mechanism of improvement on their electro-optical properties. Therefore, this study investigates the effects of H_2 plasma treatment on the structural, electrical, and optical characteristics of AZO films prepared at different substrate temperatures. The H_2 plasma treatment in this study was carried out using a plasma-enhanced chemical vapor deposition (PECVD) system because it is convenient and practical for large-area applications such as solar cells and flat-panel displays. This study also investigates the electrical stability of AZO films in air ambient.

2. Experiments

Zinc oxide powder mixed with 2 wt.% aluminum oxide was sintered to be used as a sputter target. Glass substrates (Corning 1737) with an area of 33×33 mm^2 were cleaned ultrasonically with isopropyl alcohol (IPA) and deionized (DI) water, and then dried under a blown nitrogen gas. A 13.56 MHz RF magnetron sputtering source was installed in the deposition chamber to deposit ceramic thin films. AZO films with a thickness of about 100 nm were deposited on the glass substrates at various temperatures at an RF power of 100 W. The base pressure was 5×10^{-6} Torr and the working pressure was maintained at 5×10^{-2} Torr in Ar (99.995%) gas. During deposition, the sample holder was spun at 40 revolutions per min to obtain a better uniformity. After deposition, the AZO thin films were treated by H_2 plasma at a temperature of 300 °C and an RF power of 10 W for 60 min. The deposition and post-treatment temperatures were no more than 300 °C due to compatibility with typical optoelectronic device processes in industry [15].

The structure of AZO films was examined by X-ray diffraction (XRD) (PANalytical) analysis with Cu-Kα radiation ($\lambda = 1.54056$ Å). The morphology of AZO films was observed using a field emission scanning electron microscope (FE-SEM) (JEOL, JSM–6700F) and an atomic force microscope (AFM) (Digital Instrument, NS4/D3100CL/Multimode). The resistivity, Hall mobility and carrier concentration were measured using a four-point probe apparatus (Napson, RT–70/RG–5) and the Van der Pauw method (BIO-RAD, HL5500IU). The chemical bonding states of oxygen, aluminum and zinc in AZO films were investigated using an X-ray photoelectron spectroscopy (XPS) (ULVAC-PHI, PHI 5000 Versaprobe). The content of hydrogen in AZO films was detected using secondary ion mass spectrometer (SIMS) (Cameca, IMF–6 F). The optical transmission spectrum was measured using a UV–VIS spectrometer (JASCO, V–570) in the wavelength ranging from 200 to 800 nm. The temperature of all the measurements is kept at room temperature (RT).

3. Results and discussion

3.1. Structural characterization

Fig. 1 shows the XRD spectra of the as-deposited and plasma treated AZO thin films, respectively, deposited at substrate temperatures of RT, 100, 200, and 300 °C. All patterns showed only a (0 0 2) preferential orientation along the *c* axis at a diffraction angle (2θ) near 34°, indicating a hexagonal wurtzite structure in both the as-deposited and plasma treated AZO films [23,29]. The 'survival of the fastest' model proposed by Drift explains the c-axis orientation in the AZO films [41]. The peak intensity of the as-deposited films increased as the substrate temperature increased from RT to 200 °C and then slightly decreased at 300 °C. The enhancement of c-axis orientation with increasing substrate temperature is due to an increase in the surface diffusion of the adsorbed species, and agrees with earlier studies [27]. The decrease in the peak

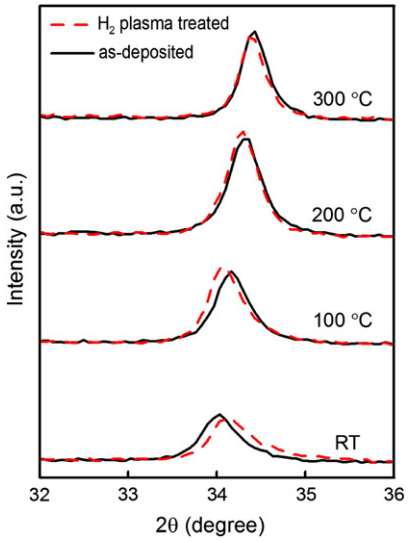

Fig. 1. XRD spectra of the as-deposited (solid line) and the hydrogen plasma treated (dotted line) AZO films.

intensity at 300 °C results from misorientation between the (0 0 2) planes and the substrate surface [42]. This result is similar to most results seen in earlier literatures [25–27,42]. Table 1 lists the parameters of the XRD patterns shown in Fig. 1. The crystalline plane distance (*d*) was estimated according to the Bragg formula: $\lambda = 2d\sin\theta$, where λ is the X-ray wavelength (1.54056 Å) and θ is the diffraction angle of the (0 0 2) peak. The lattice constant, *c*, is equal to 2*d* for the (0 0 2) diffraction peak. The strain (ε) of the films along *c*-axis is given by the equation: $\varepsilon = [(c_{film} - c_{bulk})/c_{bulk}]$, where c_{bulk} is the unstrained lattice parameter measured from bulk ZnO [26]. The diffraction angle shifted from 34.03° to 34.43° as the substrate temperature increased from RT to 300 °C. This shift in the 2θ angle is similar to, but slightly larger than, that in previous studies [25,26]. The difference between this study and earlier research may be due to different sputtering systems and deposition parameters. The crystalline plane distance and the lattice constants both decreased as the temperature increased. These results reveal that more Al atoms replaced substitutional Zn at a high deposition temperature because the ionic radii of Zn^{2+} and Al^{3+} are 72 and 53 pm, respectively [36].

For the plasma treated films, the (0 0 2) peak positions slightly shifted toward smaller diffraction angles compared than those of the untreated films at deposition temperatures ranging from 100 to 300 °C. This phenomenon indicates an increase in the interplanar distance, d_{002}. On the contrary, for films deposited at RT, results showed that the 2θ value shifted toward a higher diffraction angle after plasma treatment, indicating a decrease in d_{002}. The decreased 2θ angle for plasma treated films prepared at 100–300 °C is due to hydrogen atoms diffusing into the AZO films and occupying the Zn – O bond center [36,43]. Liu et al. [36] reported an increase in the lattice parameter of ZnO films, indicated by the smaller diffraction angle for the sample deposited with additional H_2. On the other hand, Oh et al. [29] presented that the (0 0 2) peak of the AZO films shifted towards a high diffraction angle when the sample was annealed in a hydrogen atmosphere. They explained that this is due to relaxation of the residual strain in the film during the annealing process. Cai et al. [33] treated the ZnO films with hydrogen or oxygen plasma and indicated that the ZnO crystallinity is not influenced after plasma treatment. The increase in lattice parameters caused by hydrogen incorporation competes with the relaxation of the residual strain in the film caused by thermal annealing. For a film deposited at a lower temperature (RT), the effect of strain relaxation dominates, and thus the (0 0 2) peak shifts right and d_{002} decreases. For a film deposited at higher

Table 1
Parameters of XRD patterns: 2θ, FWHM, *d*, *c* and strain of the as-deposited and the hydrogen plasma treated AZO thin films grown at different substrate temperatures.

	Substrate temperature	2θ	FWHM	*d* (nm)	*c* (nm)	Strain	Crystallite size (nm)
As-dep.	RT	34.03°	0.43°	0.26323	0.52645	1.11×10^{-2}	19.3
	100 °C	34.16°	0.41°	0.26223	0.52445	7.23×10^{-3}	20.1
	200 °C	34.37°	0.39°	0.26074	0.52148	1.52×10^{-3}	21.1
	300 °C	34.43°	0.34°	0.26025	0.52050	-3.61×10^{-4}	24.3
Plasma-treated	RT	34.16°	0.52°	0.26223	0.52445	7.23×10^{-3}	15.9
	100 °C	34.10°	0.41°	0.26273	0.52545	9.14×10^{-3}	20.0
	200 °C	34.30°	0.39°	0.26123	0.52247	3.42×10^{-3}	21.2
	300 °C	34.37°	0.32°	0.26074	0.52148	1.52×10^{-3}	25.8

temperatures (100–300 °C), the effect of hydrogen incorporation dominates, and thus the (0 0 2) peaks shift left and d_{002} increases.

Fig. 2(a)–(d) presents the FE-SEM images of the as-deposited AZO films deposited at various substrate temperatures. These figures show that the substrate temperature had a significant influence on the morphology and microstructure of AZO films. The surface grain size increased significantly as substrate temperature increased from RT to 300 °C. A higher substrate temperature provided surface adatoms with higher mobility to diffuse, thus improving the surface grain size of the film [26,44,45]. This result agrees with previous research [46,47].

Fig. 3(a)–(d) presents the FE-SEM images of the plasma treated AZO films deposited at various substrate temperatures. Compared to Fig. 2, the film surface morphology did not obviously change after plasma treatment. However, the calculated surface grain size increased slightly after H_2 plasma treatment. This phenomenon can be explained by the etching effect of small grains growing among large grains and a rearrangement of surface atoms due to the bombardment of activated hydrogen radicals. Therefore, the surface grain size of the plasma treated film appeared larger than that of the as-deposited film. Baik et al. [28] reported that the grain size of AZO film slightly increased after hydrogen treatment using photo-CVD for 30 min.

Fig. 4(a)–(d) shows the AFM images of the as-deposited and plasma treated AZO films deposited at RT and 300 °C. Table 2 shows the root mean square (RMS) roughness of the films. For the as-deposited films, the RMS roughness increased from 1.96 to 8.70 nm as the substrate temperature increased from RT to 300 °C. The rougher film is attributed to larger surface grains grown at higher substrate temperature, as Fig. 2 shows. This result is different from previous studies [26,48]. Fu et al. [48] reported that the surface roughness of the AZO film remained unchanged as the substrate temperature increased. Li et al. [26] reported that the surface roughness of the AZO films decreased as the substrate temperature increased from RT to 200 °C. They concluded that the oxygen in the plasma gas during the deposition process could cause a re-sputtering effect, thus improving film roughness. However, the experiment in this study did not use oxygen gas during the sputtering process. The RMS roughness of plasma treated AZO films increased slightly compared to the as-deposited samples, regardless of deposition temperature. This increase in surface roughness may be attributed to the etching effect of hydrogen radicals, and is consistent with the findings in Figs. 2 and 3. The AFM observations in these figures reveal that H_2 plasma treatment using a PECVD system may be an attractive method for achieving textured transparent electrodes for solar cells.

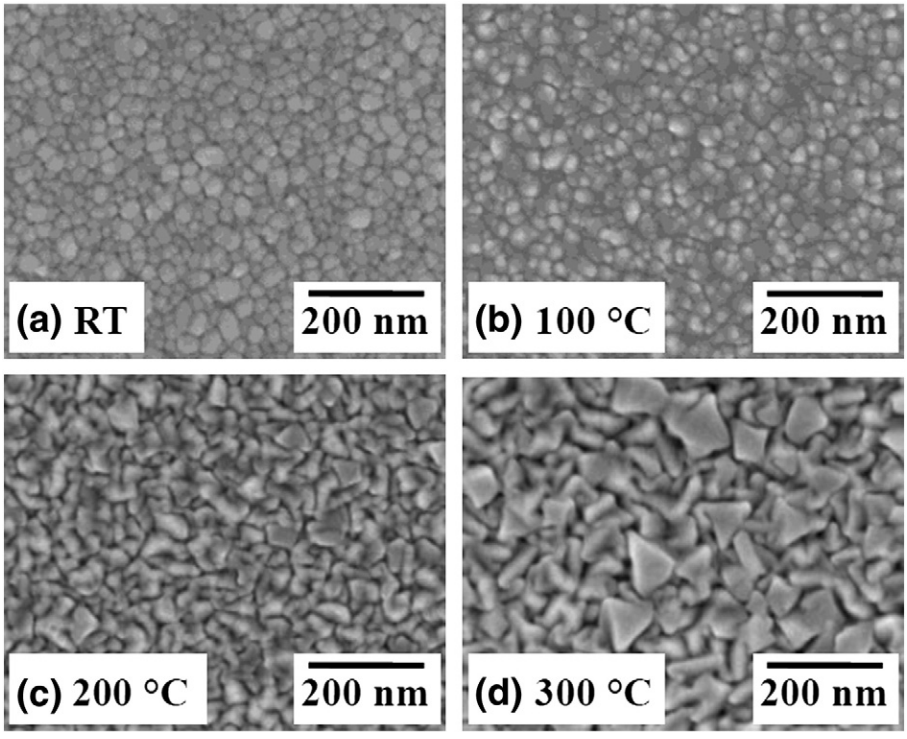

Fig. 2. SEM micrographs of the as-deposited AZO films deposited at deposition temperatures of (a) RT, (b) 100, (c) 200 and (d) 300 °C.

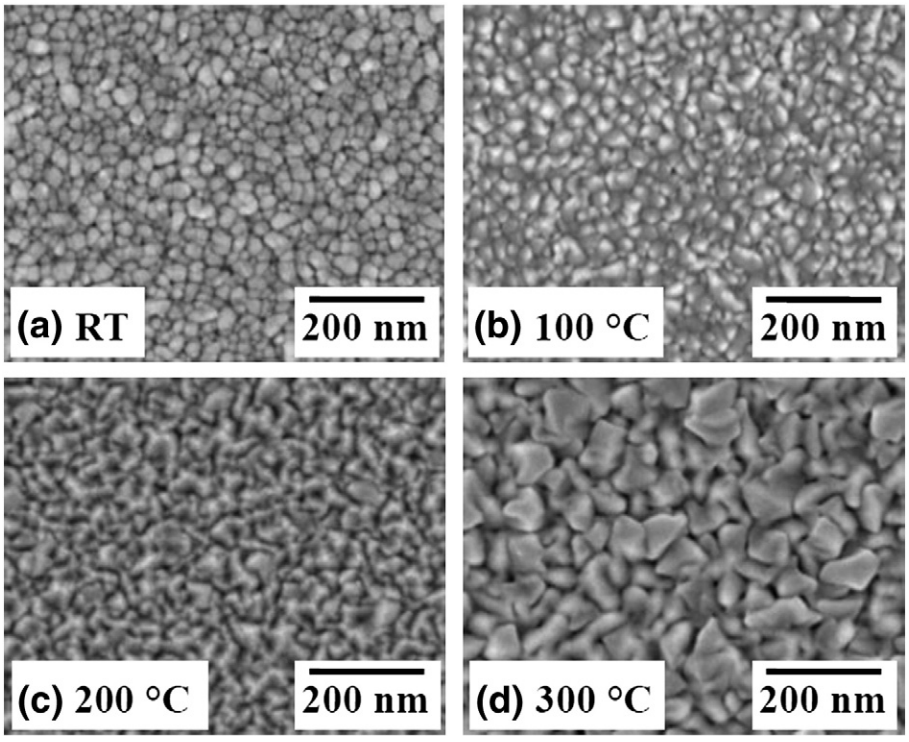

Fig. 3. SEM micrographs of the plasma treated AZO films at deposition temperatures of (a) RT, (b) 100, (c) 200, and (d) 300 °C.

3.2. Electrical properties

Fig. 5 illustrates the dependence of the electrical properties of the as-deposited and plasma treated AZO films on substrate temperature. Table 3 lists the electrical and optical properties of these films. The resistivity of the as-deposited sample decreased by two orders of magnitude when the substrate temperature increased form RT to 300 °C. The film deposited at 300 °C possessed the minimum

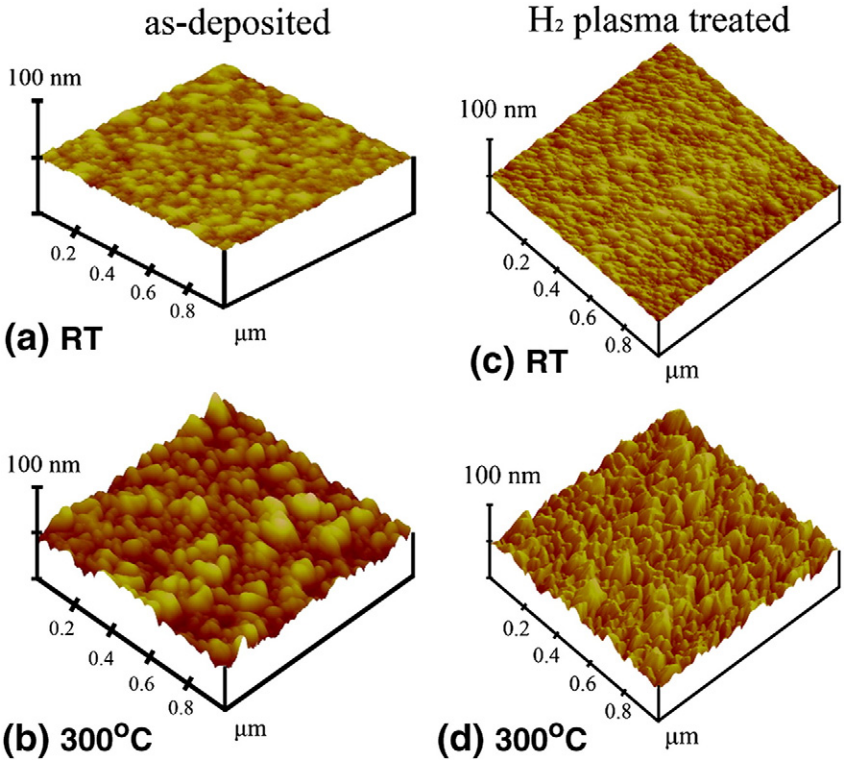

Fig. 4. AFM images of the as-deposited and the plasma treated AZO films deposited at temperatures of RT and 300 °C.

Table 2
RMS roughness of the as-deposited and the plasma treated AZO thin films deposited at different substrate temperatures.

Deposition temperature	RT	100 °C	200 °C	300 °C
As-deposited films (nm)	1.96	2.42	2.96	8.70
Plasma treated films (nm)	2.26	2.59	4.15	10.05

resistivity. The resistivities of all the plasma treated films decreased to below $3.03\times10^{-3}\ \Omega$ cm, regardless of the substrate temperature. That is, the resistivities of the plasma treated films were decreased by 97.6% to 22.7% at deposition temperatures of RT–300 °C, respectively. The improvement in resistivity was strongly dependent on the deposition temperature of AZO films. The resistivity is the combined result of the Hall mobility and the carrier concentration. In the as-deposited films, the Hall mobility and the carrier concentration both increased with the substrate temperature due to better crystallinity and more intrinsic donors at a higher deposition temperature [44]. The Hall mobility increased by 642% to 28% after plasma treatment, and the carrier concentration increased by 457% to 8.7% for the samples deposited at the substrate temperatures of RT–300 °C. These results indicate that the lower deposition temperature, the greater the improvement in the electrical characteristics of the AZO films. However, the plasma treated films deposited at high temperatures still had better electrical characteristics than those deposited at low temperatures. The increase in carrier concentration may be due to desorption of negatively charged oxygen species, which increases oxygen vacancies or interstitial zinc atoms, and the formation of shallow donors generated by incorporated hydrogen [29–31,44]. The increase in mobility for the plasma treated films may be attributed to desorption of oxygen species and passivation of acceptors and defects at grain boundaries, which decreases the barrier potential and grain boundary scattering, thus improving mobility [28,44]. These results are consistent with the previous findings [44,49].

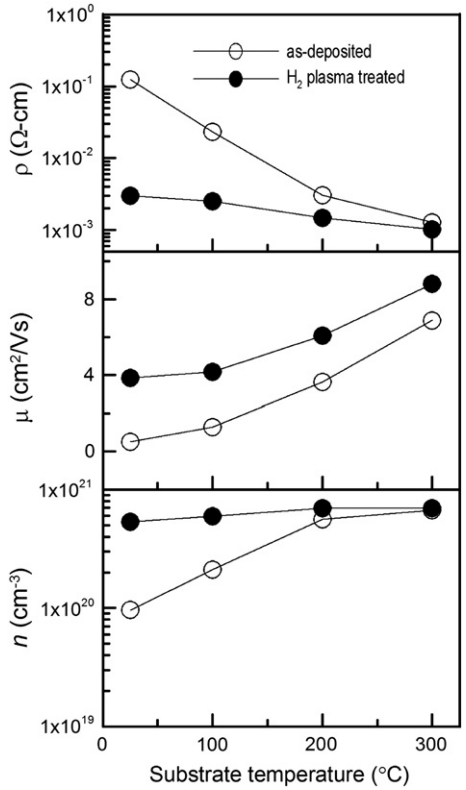

Fig. 5. Resistivity (ρ), Hall mobility (μ) and carrier concentration (n) of the AZO films as a function of the substrate temperature.

The content of hydrogen in the films was measured by SIMS to identify the hydrogen incorporation in the plasma treated AZO films Fig. 6 shows the secondary H^+ content in the as-deposited and the plasma treated AZO films as a function of etching time. Results indicate that hydrogen atoms penetrated throughout the entire AZO films and the secondary H^+ count for the plasma treated film was approximately 50% higher than that for the as-deposited film. The incorporated hydrogen atoms in the AZO films may form Zn–H–Zn and OH…O species, leading to passivation of grain boundary surfaces [2,37]. In addition, oxygen vacancy in ZnO films causes decrease of d_{002} spacing while hydrogen donor increases it [50,51]. The left shift of the (0 0 2) peak for the plasma treated AZO films in Fig. 1(b) suggests that hydrogen donors contribute to the increase of the carrier concentration more than oxygen vacancies [30]. Thus, the H_2 plasma treatment effectively improves carrier concentration and Hall mobility and reduces film resistivity.

To clarify the mechanism of the improvement in resistivity, the chemical structure of the as-deposited and the plasma treated AZO films was investigated by XPS. Fig. 7(a)–(d) shows the XPS spectra and their Gaussian-resolved components of (a) O 1s (b) Al $2p_{3/2}$ (c) Zn $2p_{3/2}$ and (d) Zn $2p_{1/2}$ for the as-deposited and plasma treated films. As Fig. 7(a) shows, the bonding states of O 1s spectra are resolved into three components centered at 530.2 ± 0.2, 531.1 ± 0.1 and 532.4 ± 0.1 eV, respectively [52]. After plasma treatment, the O 1s peaks slightly shifted to the high energy side and were located at 530.75, 531.89, and 532.71 eV. The high bonding energy component centered at 532.4 ± 0.1 eV is attributed to the existence of negatively charged oxygen species, such as $-CO_3$, $-OH$, adsorbed H_2O or adsorbed O_2, on the surfaces of the AZO films [52,53]. After plasma treatment, the area ratio of the high energy peak decreased from 24.4% to 14.7%, indicating desorption of the negatively charged oxygen species from the film during the plasma exposure. This result would increase the carrier concentration in the plasma treated AZO films. The low bonding energy component centered at 530.2 ± 0.2 eV is attributed to O^{2-} ions on the wurtzite structure of the hexagonal Zn^{2+} ion array, surrounded by Zn atoms with their full complement of nearest neighbor O^{2-} ions [52]. After plasma treatment, the area ratio of the low energy component increased from 22.3% to 28.8%, indicating an increase in the amount of oxygen atoms in a fully oxidized stoichiometric surrounding. The medium bonding energy component centered at 531.1 ± 0.1 eV is attributed to O^{2-} ions in the oxygen deficient region within the ZnO matrix [54]. After plasma treatment, the area ratio of the medium energy component increased from 53.3% to 56.5%, indicating an increase in the concentration of oxygen vacancies in the films. This result also contributed to the increase of the carrier concentration in the plasma treated films. Oh. et al. [54] reported that the area ratio of the low bonding energy component increased and the area ratio of the high bonding energy component decreased when the AZO film was annealed in H_2 atmosphere at 300 °C for 1 h. However, the phenomenon that the area ratio of the medium bonding energy component remained unchanged after hydrogen annealing is different from the current results.

Fig. 7(b) shows the XPS data of the Al $2p_{3/2}$ for the as-deposited and the plasma treated AZO films. The low binding energy component centered at 72.7 ± 0.1 eV is due to the presence of metallic Al [37,52]. After plasma treatment, the area ratio of this component decreased from 21.7% to 13.7%, indicating that metallic Al decreased and segregated at the grain boundaries. The high bonding energy component centered at 73.7 ± 0.1 eV suggests an oxygen-deficiency in the ZnO matrix [52]. This energy component is slightly shifted toward a lower binding energy than 74.6 eV, the peak position of stoichiometric Al_2O_3. After plasma treatment, the area ratio of this component increased from 78.3% to 86.3%, indicating that more Al atoms were bound to O ions as a result of the plasma exposure.

Fig. 7(c) and (d) presents the XPS data of the Zn $2p_{3/2}$ and the Zn $2p_{1/2}$ for the AZO films, respectively. The Zn $2p_{3/2}$ peak can be split

Table 3
Resistivity, Hall mobility, carrier concentration, average transmittance, and optical bandgap of the as-deposited and the hydrogen plasma treated AZO thin films deposited at different substrate temperatures.

	Deposition temperature (°C)	Resistivity (Ω cm)	Hall mobility (cm^2/V s)	Carrier concentration (cm^{-3})	Average transmittance (%)	Optical bandgap (eV)
As-dep.	RT	1.25×10^{-1}	0.52	9.61×10^{19}	81.0	3.345
	100	2.33×10^{-2}	1.27	2.11×10^{20}	81.1	3.365
	200	3.07×10^{-3}	3.63	5.60×10^{20}	82.5	3.420
	300	1.32×10^{-3}	6.89	6.89×10^{20}	85.0	3.520
Plasma-treated	RT	3.03×10^{-3}	3.86	5.35×10^{20}	82.6	3.421
	100	2.53×10^{-3}	3.26	7.59×10^{20}	83.8	3.440
	200	1.47×10^{-3}	6.07	6.99×10^{20}	82.2	3.484
	300	1.02×10^{-3}	8.80	6.95×10^{20}	84.9	3.531

into two components at 1021.2 eV and 1022.2 eV. The low bonding energy component is due to the presence of metallic Zn and the high bonding energy component exhibits the Zn in the oxidized state (Zn–O) [52]. After plasma treatment, the area ratios of these components remained almost unchanged. However, their bonding energies shifted slightly toward the higher energy side. The Zn $2p_{1/2}$ peak can be split into two components at 1044.4 (metallic Zn) and 1045.4 eV (Zn–O). The area ratio of the low bonding energy component almost disappeared in the plasma treated films, and both components shifted slightly toward the high energy side as compared to the as-deposited films. The right shift of the bonding energy component reveals formation of Zn–H bonds [51,55]. These results agree with the observations in Figs. 1 and 5.

This study investigates film resistivity as a function of air exposure time to determine the electrical stability of the AZO films, as Fig. 8 shows. Results showed that the resistivities of all films gradually deteriorated when exposed to air ambient for 500 h. A lower deposition temperature led to increased aging deterioration. The film deposited at a lower temperature had a smaller grain size and greater defect density on the grain boundary surface, which obstructed carrier transport when the AZO film was exposed to air ambient [54]. Moreover, the plasma treated films exposed to air ambient for 500 h exhibited better electrical stability than the as-deposited films. This result supports that H_2 plasma treatment may passivate the grain boundary surface and suppress the generation of oxygen species, leading to better electrical stability in the AZO films.

3.3. Optical properties

Fig. 9(a) and (b) shows the optical transmittance spectra of the as-deposited and plasma treated AZO films, respectively, at various deposition temperatures. All films had high transmittances in the visible region (400–700 nm) and a strong absorption in the UV region.

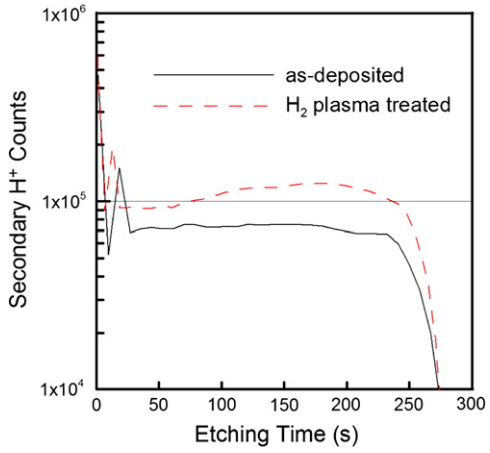

Fig. 6. Secondary H^+ content in the AZO films as a function of etching time.

The average transmittances of the as-deposited films, as Table 3 listed, slightly increased with the deposition temperatures. The increase of optical transmittance with increasing deposition temperature can be attributed to the weakening of scattering and absorption of light due to better crystallinity and a flatter film surface. Li et al. [26] reported that the optical transmittance of the AZO films deposited by DC reactive magnetron sputtering increased slightly with the deposition temperature. The defects in grain boundaries also decreased [26]. After plasma treatment, the transmittance of the AZO films deposited at low substrate temperatures (RT–100 °C) increased, while those deposited at high substrate temperatures (200–300 °C) did not vary significantly. Chung et al. [37] reported that AZO:H films had better transmittance than AZO films at a sputtering temperature of 50 °C. The absorption edges for the plasma treated samples shifted toward the short wavelength side more than those without plasma treatment did.

The dependence of optical absorption coefficient (α) on photon energy ($h\nu$) was examined to determine optical bandgap energy (E_g) of the AZO films [56]. Fig. 10(a) and (b) shows the graph of α^2 vs. photon energy for the as-deposited and plasma treated AZO films, respectively. The calculated E_g values, as Table 3 listed, ranged from 3.345 to 3.520 eV for the as-deposited AZO films. The film deposited at a higher temperature exhibited a stronger blue shift phenomenon. Fig. 10(b) shows that the E_g values ranged from 3.421 to 3.531 eV for the plasma treated samples. In contrast to the as-deposited films, the E_g of the plasma treated samples broadened and even more so for films deposited at a lower temperature. The broadening in the bandgap was known as the Burstein–Moss effect [57]. The following equation shows that the bandgap widening (ΔE_g) is related to carrier concentration (n_e) in a degenerate semiconductor:

$$\Delta E_g = \frac{h^2}{8m^*}\left(\frac{3}{\pi}\right)^{2/3} {n_e}^{2/3}, \tag{1}$$

where h is Planck's constant and m^* is the electron effective mass in conduction band. E_g broadening supports the previous result that the carrier concentration of the AZO film is increased after hydrogen plasma treatment, as Fig. 5 shows.

Fig. 11 shows the blueshift (ΔE_g) as a function of carrier concentration for the as-deposited and plasma treated AZO films. It was found that ΔE_g was approximately proportional to n_e. To estimate the relation between ΔE_g and n_e quantitatively, set $m^* = 0.28\ m_0$, where m_0 is the free electron mass [58] and substitute measured values of ΔE_g and n_e into Eq. (1). The calculated corresponding exponent is about 0.64 for all the AZO films regardless of plasma treatment, which approximately follows Eq. (1). Oh et al. [20] also reported that the exponent is 0.655 from their Burstein–Moss shift measurement of the AZO films. However, other research [27,59] shows that the exponent was in the range from 1/3 to 2/3. They explained that the electronic state of the films can be calibrated by electron–electron or electron-impurity scattering as the film has a high carrier concentration (~10^{20} cm^{-3}). Namely, the many-body effect

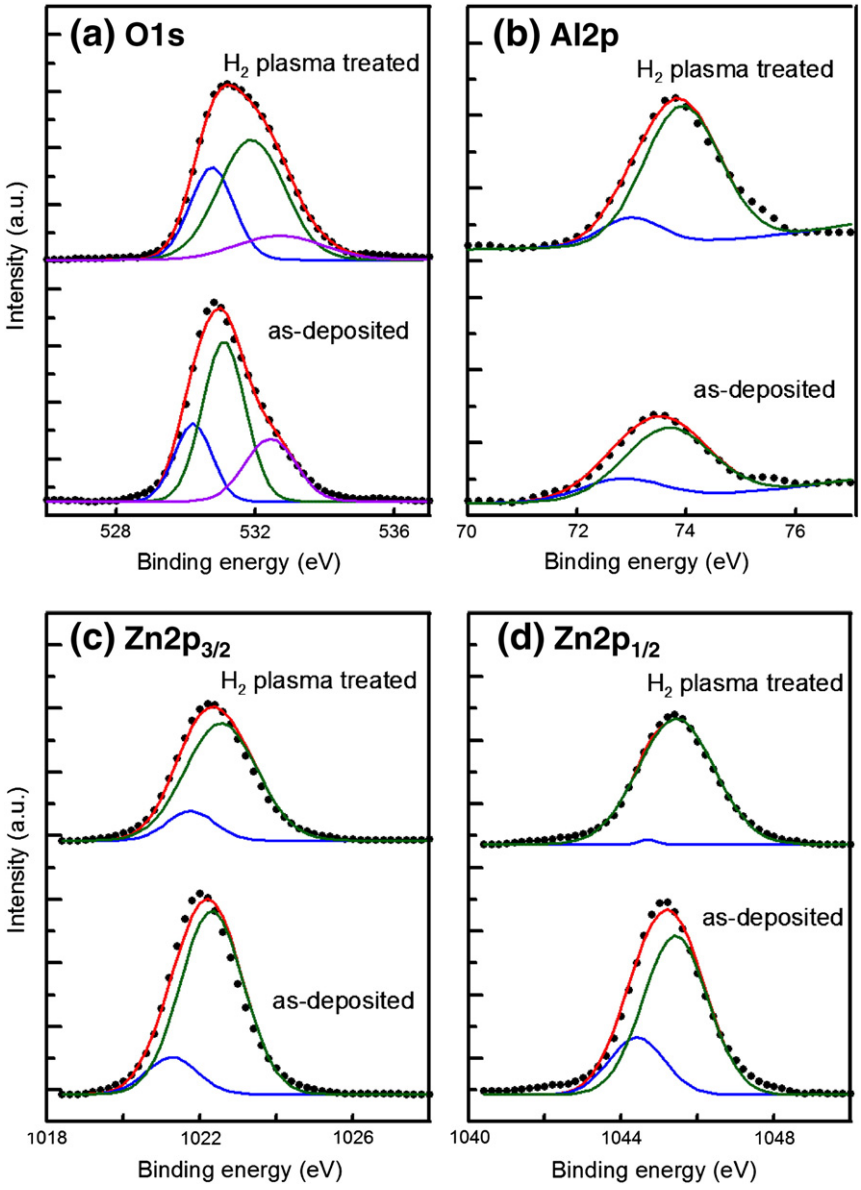

Fig. 7. XPS spectra and their Gaussian-resolved components of (a) O 1 s (b) Al $2p_{3/2}$ (c) Zn $2p_{3/2}$ and (d) Zn $2p_{1/2}$ for the as-deposited and the plasma treated AZO films.

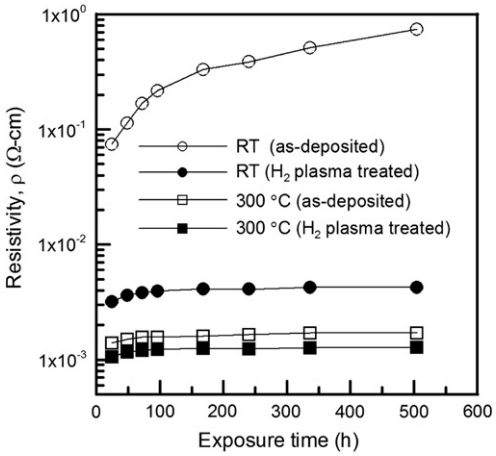

Fig. 8. Resistivity of (a) the as-deposited and (b) the plasma treated AZO films as a function of the air exposure time.

such as Coulomb interaction or exchange interaction makes the bandgap decrease [27]. Obviously, such a scattering phenomenon is slight in our developed AZO films.

4. Conclusions

This study demonstrates the effects of H_2 plasma treatment on properties of the AZO thin film deposited by RF magnetron sputtering on glass substrates at different substrate temperatures ranging from RT to 300 °C. The H_2 plasma treatment did not significantly change the crystallinity of the film but slightly increased its surface roughness and surface grain size. The H_2 plasma treatment markedly improved film resistivity. The resistivities decreased by from 22.7% to 97.6% as the deposition temperature fell from 300 °C to RT. The plasma treated film deposited at 300 °C achieved the minimum resistivity of $1.02\times10^{-3}\ \Omega$ cm. The H_2 plasma treatment improved the aging deterioration phenomenon in air. Moreover, the optical transmittances of the AZO films with low deposition temperatures (RT–100 °C) increased slightly by 2%–3%, while those with a high deposition temperatures (200–300 °C) did not change markedly

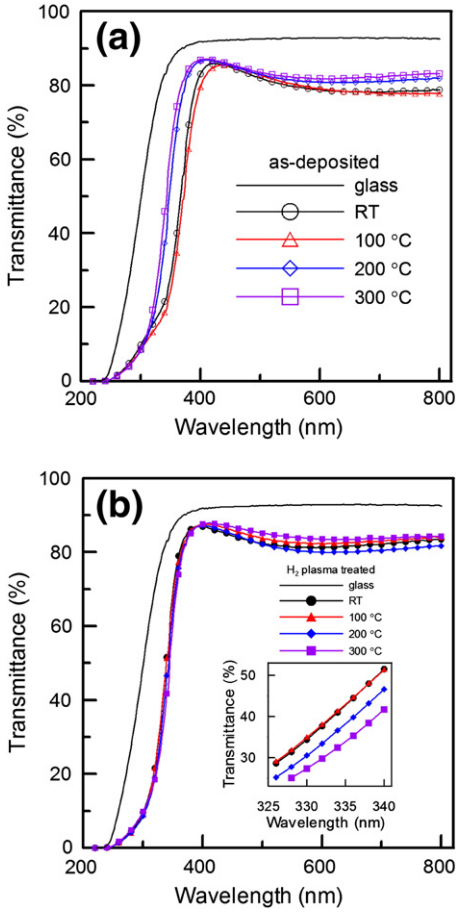

Fig. 9. Optical transmittance spectra of (a) the as-deposited AZO films and (b) the plasma treated AZO films with various substrates temperatures.

after plasma treatment. The plasma treatment also caused E_g broadening and ΔE_g increased monotonically from 0.011 to 0.076 eV as the deposition temperature decreased from 300 °C to RT. The E_g broadening in all the AZO films is proportional to a 0.64 power of the

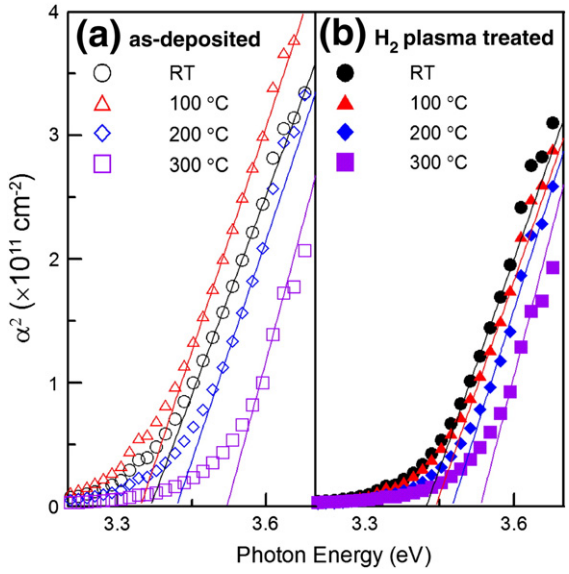

Fig. 10. Plot of α^2 versus photon energy for the as-deposited and plasma treated AZO films.

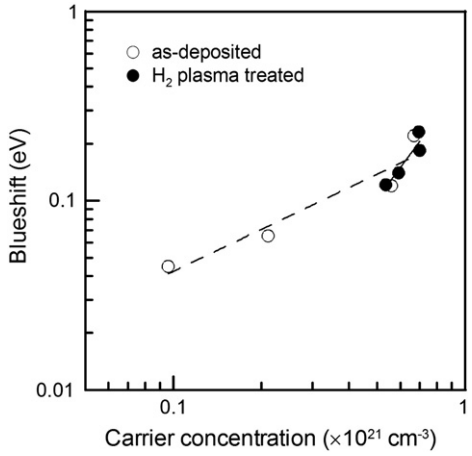

Fig. 11. Blueshift (the difference of the bandgap between AZO and ZnO film) as a function of carrier concentration for the as-deposited and the plasma treated AZO films.

carrier concentration. The improved electrical properties of the plasma treated AZO films were ascribed to the incorporated hydrogen atoms acting as shallow donors and passivating surface and defects at the grain boundaries and the desorption of negative charged oxygen species at the grain boundaries.

Acknowledgments

The authors would like to thank the National Science Council of the Republic of China (Taiwan), for partly financially support under contract No. NSC 95-2221-E-005-111.

References

[1] R.G. Gordon, MRS Bull. 25 (8) (2000) 52.
[2] S. Major, S. Kumar, M. Bhatnagar, K.L. Chopra, Appl. Phys. Lett. 49 (1986) 394.
[3] L. Kerkache, A. Layadi, A. Mosser, J. Alloys Compd. 485 (2009) 46.
[4] S.H. Paeng, M.W. Park, Y.M. Sung, Surf. Coat. Technol. 205 (2010) S210.
[5] M. Purica, E. Budianu, E. Rusu, M. Danila, R. Gavrila, Thin Solid Films 403–404 (2002) 485.
[6] V. Khranovskyy, J. Eriksson, A. Lloyd-Spetz, R. Yakimova, L. Hultman, Thin Solid Films 517 (2009) 2073.
[7] S.Y. Myong, K.S. Lim, Appl. Phys. Lett. 82 (2003) 3026.
[8] M.A. Martinez, J. Herrero, M.T. Gutierrez, Sol. Energy Mater. Sol. Cells 45 (1997) 75.
[9] N. Sakai, Y. Umeda, F. Mitsugi, T. Ikegami, Surf. Coat. Technol. 202 (2008) 5467.
[10] F. Richter, T. Welzel, R. Kleinhempel, T. Dunger, T. Knoth, M. Dimer, F. Milde, Surf. Coat. Technol. 204 (2009) 845.
[11] G.G. Valle, P. Hammer, S.H. Pulcinelli, C.V. Santilli, J. Eur. Ceram. Soc. 24 (2004) 1009.
[12] H.M. Ali, M.M. Abd El-Raheem, N.M. Megahed, H.A. Mohamed, J. Phys Chem. Solids 67 (2006) 1823.
[13] L. Gong, Z. Ye, J. Lu, L. Zhu, J. Huang, X. Gu, B. Zhao, Vacuum 84 (2010) 947.
[14] H.P. Lobl, M. Huppertz, D. Mergel, Surf. Coat. Technol. 82 (1996) 90.
[15] L.S. Wang, G.H. Yue, Y.Z. Chen, R.T. Wen, X. Wang, D.L. Peng, Mater. Chem. Phys. 117 (2009) 224.
[16] S.T. Kuo, W.H. Tuan, Y.W. Lao, C.K. Wen, H.R. Chen, Int. J. Appl. Ceram. Technol. 6 (2009) 223.
[17] Q. Zhao, T. Cai, S. Wang, R. Zhu, Z. Liao, D. Yu, Appl. Phys. A 100 (2010) 165.
[18] S. Roy, S. Basu, Bull. Mater. Sci. 25 (2002) 513.
[19] D.T. Phan, G.S. Chung, Appl. Surf. Sci. 257 (2011) 4339.
[20] B.Y. Oh, M.C. Jeong, W. Lee, J.M. Myoung, J. Cryst Growth 274 (2005) 453.
[21] B. Houng, C.J. Huang, Surf. Coat. Technol. 201 (2006) 3188.
[22] S. Takata, T. Minami, H. Nanto, Thin Solid Films 135 (1986) 183.
[23] H. Agura, A. Suzuki, T. Matsushita, T. Aoki, M. Okuda, Thin Solid Films 445 (2003) 263.
[24] T. Minami, H. Sato, H. Nanto, S. Takata, Jpn. J. Appl. Phys. 24 (1985) L781.
[25] K.C. Park, D.Y. Ma, K.H. Kim, Thin Solid Films 305 (1997) 201.
[26] X.Y. Li, H.J. Li, Z.J. Wang, H. Xia, Z.Y. Xiong, J.X. Wang, B.C. Yang, Opt. Commun. 282 (2009) 247.
[27] K.H. Kim, K.C. Park, D.Y. Ma, J. Appl. Phys. 81 (1997) 7764.
[28] S.J. Baik, J.H. Jang, C.H. Lee, W.Y. Cho, K.S. Lim, Appl. Phys. Lett. 70 (1997) 3516.
[29] B.Y. Oh, M.C. Jeong, D.S. Kim, W. Lee, J.M. Myoung, J. Cryst. Growth 281 (2005) 475.
[30] N. Ohashi, Y.G. Wang, T. Ishigaki, Y. Wada, H. Taguchi, I. Sakaguchi, T. Ohgaki, Y. Adachi, H. Haneda, J. Cryst. Growth 306 (2007) 316.

[31] Y.M. Strzhemechny, H.L. Mosbacker, D.C. Look, D.C. Reynolds, C.W. Litton, N.Y. Garces, N.C. Giles, L.E. Halliburton, S. Niki, L.J. Brillson, Appl. Phys. Lett. 84 (2004) 2545.
[32] R. Das, T. Jana, S. Ray, Sol. Energy Mater. Sol. Cells 86 (2005) 207.
[33] P.F. Cai, J.B. You, X.W. Zhang, J.J. Dong, X.L. Yang, Z.G. Yin, N.F. Chen, J. Appl. Phys. 105 (2009) 083713.
[34] T. Ishigaki, N. Ohashi, H. Taguchi, R. Ye, H. Haneda, S. Ito, Thin Solid Films 506–507 (2006) 303.
[35] Z. Zhou, K. Kato, T. Komaki, M. Yoshino, H. Yukawa, M. Morinaga, K. Morita, J. Eur. Ceram. Soc. 24 (2004) 139.
[36] W.F. Liu, G.T. Du, Y.F. Sun, J.M. Bian, Y. Cheng, T.P. Yang, Y.C. Chang, Y.B. Xu, Appl. Surf. Sci. 253 (2007) 2999.
[37] Y.M. Chung, C.S. Moon, W.S. Jung, J.G. Han, Thin Solid Films 515 (2006) 567.
[38] S.H. Lee, T.S. Lee, K.S. Lee, B. Cheong, Y.D. Kim, W.M. Kim, J. Phys. D: Appl. Phys. 41 (2008) 095303.
[39] H.P. Chang, F.H. Wang, J.Y. Wu, C.Y. Kung, H.W. Liu, Thin Solid Films 518 (2010) 7445.
[40] F.H. Wang, H.P. Chang, C.C. Tseng, C.C. Huang, H.W. Liu, Curr. Appl. Phys. 11 (2011) s12.
[41] A. Van der Drift, Philips Res. Rep. 22 (1967) 267.
[42] S. Singh, R.S. Srinivasa, S.S. Major, Thin Solid Films 515 (2007) 8718.
[43] L.Y. Chen, W.H. Chen, J.J. Wang, F.C.N. Hong, Y.K. Su, Appl. Phys. Lett. 85 (2004) 5628.
[44] G. Fang, D. Lia, B.L. Yao, Vacuum 68 (2003) 363.
[45] K.H. Kim, R.A. Wibowo, B. Munir, Mater. Lett. 60 (2006) 1931.
[46] J.K. Kim, S.J. Yun, J.M. Lee, J.W. Lim, Curr. Appl. Phys. 10 (2010) S451.
[47] D. Song, P. Widenborg, W. Chin, A.G. Aberle, Sol. Energy Mater. Sol. Cells 73 (2002) 1.
[48] E.G. Fu, D.M. Zhuang, G. Zhang, Z. Ming, W.F. Yang, J.J. Liu, Microelectronics J. 35 (2004) 383.
[49] C.H. Seager, S.M. Myers, J. Appl. Phys. 94 (2003) 2888.
[50] Y.E. Lee, J.B. Lee, Y.J. Kim, H.K. Yang, J.C. Park, H.J. Kim, J. Vac. Sci. Technol. A 14 (1996) 1943.
[51] C.G. Van de Walle, Phys. Rev. Lett. 85 (2000) 1012.
[52] M. Chen, X. Wang, Y.H. Yu, Z.L. Pei, X.D. Bai, C. Sun, R.F. Huang, L.S. Wen, Appl. Surf. Sci. 158 (2000) 134.
[53] H. Sato, T. Minami, S. Takata, T. Mouri, N. Ogawa, Thin Solid Films 220 (1992) 327.
[54] B.Y. Oh, M.C. Jeong, J.M. Myoung, Appl. Surf. Sci. 253 (2007) 7157.
[55] J. Cho, K.H. Yoon, M.S. Oh, W.K. Choi, J. Electrochem. Soc. 150 (2003) H225.
[56] J.F. Chang, M.H. Hon, Thin Solid Films 386 (2001) 79.
[57] E. Burstein, Phys. Rev. 93 (1954) 632.
[58] B.E. Serne us, K.F. Berggren, Z.C. Jim, I. Hamberg, C.G. Granqvist, Phys. Rev. B. 37 (1988) 10244.
[59] B.H. Choi, H.B. Im, J.S. Song, K.H. Yoon, Thin Solid Films 193/194 (1990) 712.